

Magnetic-field-inhomogeneity-induced transverse-spin relaxation of gaseous ^{129}Xe in a cubic cell with a stem

Deok-Young Lee^{✉,*}, Sangkyung Lee^{✉,†}, M. M. Kim[✉], and Sin Hyuk Yim
 Agency for Defense Development, Daejeon 34186, Republic of Korea

 (Received 20 January 2021; revised 1 October 2021; accepted 4 October 2021; published 27 October 2021)

We investigate the transverse-spin relaxations of ^{129}Xe due to diffusion in the presence of magnetic-field gradients in relation to the dimensions of a sub-cm sized cubicle atomic gas cell with a stem. The transverse-spin-relaxation rate ($\Gamma_{\Delta B}$) of ^{129}Xe is measured as a function of various magnetic-field gradients, $\partial B_z/\partial x$, $\partial B_z/\partial y$, $\partial B_z/\partial z$, and $\partial B_y/\partial y$. From the measured transverse-spin-relaxation rates in five atomic gas cells with different stem sizes, the quadratic coefficients of $\Gamma_{\Delta B}$ with respect to the magnetic-field gradients are extracted. To investigate the effect of the dimensions of the stem, we calculate the ratio between the quadratic coefficients in each atomic gas cell, which is invariant under scaling in the cell size and change in the diffusion coefficient. We compare these ratios with those obtained analytically from a rectangular parallelepiped model for the atomic gas cells and with those obtained numerically from a more precise model taking the stems directly into account. Using a scaling argument, we provide a scheme for estimating the quadratic coefficient of a cubic atomic cell with a stem. Finally, we determine the diffusion coefficient from the measured quadratic coefficient. Compared to the analytical method for a rectangular parallelepiped, numerical analysis considering the stem provides the diffusion coefficient as a value close to the value given by Fuller's equation. We estimate the diffusion coefficients of ^{129}Xe in the gas mixture of nitrogen, ^{129}Xe , and ^{131}Xe as $0.13 \text{ cm}^2/\text{s}$ at the standard temperature and pressure condition.

DOI: [10.1103/PhysRevA.104.042819](https://doi.org/10.1103/PhysRevA.104.042819)

I. INTRODUCTION

Noble gas atoms have been widely applied to MRI [1–3], gyroscopes [4], magnetometers [5], and even fundamental symmetry tests [6,7], which rely on their long spin-relaxation times. These usually range from minutes to hours, depending on the atom. Among noble gases, xenon is suitable for gyroscopes because of its “Goldilocks” spin-exchange cross section [8]. It has a moderate spin-relaxation time, on the order of 100 s, which means that its spin can be initialized after a relatively short time compared to other noble gas atoms. Spin-relaxation times can be classified into two categories, longitudinal-spin-relaxation time T_1 and transverse-spin-relaxation time T_2 . In this paper, T_2 represents the effective macroscopic transverse relaxation time including the dephase effect due to the field inhomogeneity, referred to as T_2^* in NMR literature [9]. The longitudinal-spin-relaxation time T_1 is related to the spin-exchange rate, determining the initialization time. The transverse-spin-relaxation time T_2 is related to the duration of the macroscopic spin precession, which determines the angular random walk of a gyroscope which is proportional to $1/T_2$ [4].

The transverse relaxation time T_2 is usually shortened by magnetic-field gradients as well as interatomic collisions and wall collisions. It can be written as the inverse of the trans-

verse relaxation rate Γ_{tot} , where $\Gamma_{\text{tot}} = \Gamma_{\text{col}} + \Gamma_{\text{wall}} + \Gamma_{\Delta B}$. Γ_{col} is the relaxation rate due to collisions between atoms, Γ_{wall} is the relaxation rate due to collisions with walls, and $\Gamma_{\Delta B}$ is the relaxation rate due to magnetic-field gradients originating from coils and the optical pumping beam. Usually, $\Gamma_{\Delta B}$ mainly contributes to the transverse-spin-relaxation rate; the diffusive motion of noble gas atoms in magnetic-field gradients causes spin phase decoherence and transitions between spin states [10]. Magnetic-field-gradient-induced spin relaxation in highly symmetric cells, such as spherical cells and cubic cells, previously has been studied [10–15]. In a spherical cell of radius R , the transverse relaxation rate is given by

$$\Gamma_{\Delta B, \text{spherical}} \approx \frac{8\gamma^2 R^4}{175D} |\nabla B_z|^2, \quad (1)$$

where γ is the gyromagnetic ratio of the noble gas atoms, D is the diffusion coefficient, and $\partial B_z/\partial z$ is the magnetic-field gradient of B_z along the longitudinal direction [10]. In a cubic cell of side length L , the transverse relaxation rate is given by [11]

$$\Gamma_{\Delta B, \text{cubic}} \approx \frac{\gamma^2 L^4}{120D} |\nabla B_z|^2. \quad (2)$$

The diffusion coefficients of noble gas atoms have been measured using Eq. (1) in cm-sized atomic gas cells where the effect of the stem is negligible [12,15].

In terms of miniaturization and low power consumption, atomic gas cells in mm size have been increasingly used in various devices and instruments [16]. Atomic gas cells

*Present address: Department of Physics, Korea Advanced Institute of Science and Technology, Daejeon 34141, Republic of Korea.

†Corresponding author: sklee82@add.re.kr

for gyroscopes which are usually pinched off using a gas torch, however, have their stems filled in with alkali-metal atoms, noble gas atoms, and buffer gas. A recently developed method of fabricating atomic gas cells for gyroscopes, which combines glass blowing and micro-electromechanical systems (MEMS) [17], also leaves a cylindrical reservoir for supplying alkali-metal vapors. In small atomic gas cells, the effect of the dimensions of the extra volume on $\Gamma_{\Delta B}$ is not negligible, so that Eq. (2) is insufficient to describe $\Gamma_{\Delta B}$. Additionally, in order to determine the diffusion coefficient in a sub-cm sized atomic gas cell by using the $\Gamma_{\Delta B}$ measurement, it has to be modified taking into account the dimension of the stem. We have studied the effect of the dimensions of the stem on $\Gamma_{\Delta B}$.

In this paper, we investigate $\Gamma_{\Delta B}$ as a function of magnetic gradients $\partial B_z/\partial x$, $\partial B_z/\partial y$, $\partial B_z/\partial z$, and $\partial B_y/\partial y$ in five different atomic gas cells to determine the dependence of $\Gamma_{\Delta B}$ on cell dimension. The quadratic coefficients of $\Gamma_{\Delta B}$ with respect to magnetic-field gradients are extracted experimentally and compared to the results of calculations based on a rectangular parallelepiped model for the cells. A numerical analysis of the spatial eigenmodes corresponding to a model which directly incorporates the stems is also performed. Based on this numerical analysis and a scaling argument, we provide an estimation for the quadratic coefficient of an atomic gas cell with a stem. By considering the dimensions of the atomic gas cells, the diffusion coefficients of Xe, on the order of sub-cm²/s, are determined from the extracted quadratic coefficients.

II. THEORY

To obtain the transverse relaxation rate resulting from a magnetic-field inhomogeneity, we follow the theory described in Ref. [10]. The Hamiltonian of the noble gas atom interacting with the magnetic field is

$$H = g_K \mu_B \vec{K} \cdot [\vec{B}_h + \vec{B}_{\text{inh}}(\vec{r})] = H^0 + H^1, \quad (3)$$

where g_K is the g -factor of the noble gas atom (i.e., $\gamma = \frac{e}{2m_p} g_K$), μ_B is the Bohr magneton, and \vec{K} is the nuclear spin operator. We assume that the homogeneous magnetic field is along the z direction, i.e., $\vec{B}_h = B_0 \hat{z}$. $\vec{B}_{\text{inh}}(\vec{r})$ is the inhomogeneous fluctuation of the magnetic field, with a mean value of nearly zero. Under the assumption that $|B_0| \gg |\vec{B}_{\text{inh}}|$, the inhomogeneous term can be treated as a perturbation. The time evolution of the system including diffusion is described by the density matrix equation:

$$\frac{\partial \rho}{\partial t} = \frac{1}{i\hbar} [H, \rho] + D \nabla^2 \rho, \quad (4)$$

where D is the diffusion coefficient which is nearly constant in the cell. D depends on the temperature of the gas and is usually on the order of sub-cm²/s at atmospheric pressure and room temperature. For calculation, the density matrix can be represented by the ansatz

$$\rho = \sum_i P_i R_i(\vec{r}) e^{-\Gamma t}. \quad (5)$$

Here, the possibly complex constant Γ represents the decay rate and the spatial functions $R_i(\vec{r})$ satisfy the boundary condition $\frac{\partial R}{\partial n} = \vec{n} \cdot \nabla R = 0$ which corresponds to nonrelaxing walls where \vec{n} is the outer unit normal. P_i are the eigenpolarizations

of the unperturbed Hamiltonian H_0 , i.e., $[H_0, P_i] = \hbar \Lambda_i P_i$. For a $K = 1/2$ system (e.g., ¹²⁹Xe), these are given by

$$P_{00} = \frac{1}{\sqrt{2}} \left(\left| \frac{1}{2} \right\rangle \left\langle \frac{1}{2} \right| + \left| -\frac{1}{2} \right\rangle \left\langle -\frac{1}{2} \right| \right), \quad \Lambda_{00} = 0, \quad (6a)$$

$$P_{10} = \frac{1}{\sqrt{2}} \left(\left| \frac{1}{2} \right\rangle \left\langle \frac{1}{2} \right| - \left| -\frac{1}{2} \right\rangle \left\langle -\frac{1}{2} \right| \right), \quad \Lambda_{10} = 0, \quad (6b)$$

$$P_{11} = \left| \frac{1}{2} \right\rangle \left\langle -\frac{1}{2} \right|, \quad \Lambda_{11} = \frac{g_K \mu_B B_0}{\hbar}, \quad (6c)$$

$$P_{1-1} = \left| -\frac{1}{2} \right\rangle \left\langle \frac{1}{2} \right|, \quad \Lambda_{1-1} = -\frac{g_K \mu_B B_0}{\hbar}, \quad (6d)$$

where P_i are orthonormalized.

The eigenvalue problem $\nabla^2 \phi(\vec{r}) + k^2 \phi(\vec{r}) = 0$ with the boundary condition $\frac{\partial \phi}{\partial n} = 0$ has an orthonormal spatial basis ($\phi = \phi_\alpha$, $k = k^{(\alpha)}$) where α denotes the mode number of the spatial modes and each $k^{(\alpha)} \geq 0$ is nondecreasing in α .

In order to solve the density-matrix equation approximately, we apply a perturbation as $\Gamma = \sum_n \Gamma^{(n)} \eta^n$ and $R_i = \sum_n R_i^{(n)} \eta^n$ where η is a perturbation parameter. Substituting these series expansions into (4) and equating the like powers of η , we get a sequence of partial differential equation (PDE) for each power of η . With a parameter g having one of the polarization index i values, and each α , it can be shown that the following ($f_{i;\alpha g}^{(0)}$, $\Gamma_{\alpha g}^{(0)}$) satisfies the zeroth-order PDE:

$$f_{i;\alpha g}^{(0)} = \phi_\alpha \delta_{ig}, \quad \Gamma_{\alpha g}^{(0)} = D(k^{(\alpha)})^2 + i\Lambda_g. \quad (7)$$

Calculating the higher-order terms upon these unperturbed initial values we conclude $\Gamma_{0g}^{(1)} = 0$ from the fact that \vec{B}_{inh} has mean zero, and the second-order term is given as follows:

$$\Gamma_{0g}^{(2)} = \sum_{\beta, j} \frac{\langle 0 | H_{gj}^1 | \beta \rangle \langle \beta | H_{jg}^1 | 0 \rangle}{\hbar^2 (\Gamma_{\beta j}^{(0)} - \Gamma_{0g}^{(0)})}, \quad (8)$$

where $H_{ij}^1 = \text{tr}(P_i^\dagger [H^1, P_j])$ and the summation is over indices β, j such that $\Gamma_{\beta j}^{(0)} \neq \Gamma_{0g}^{(0)}$. β denotes the mode number of the spatial modes, j denotes the index of eigenpolarization, and the bra-kets denote the spatial integration.

The above discussion shows that calculating the spatial modes in an atomic gas cell is required to predict the transverse-spin-relaxation rate. Our cell can be subdivided into a cubic part (the primary component) and a rectangular parallelepiped part (stem), as shown in Fig. 1(a). When the inner widths of the stems d are comparable to the inner lengths of the cubic parts L , we can regard an atomic gas cell as a single rectangular parallelepiped with side lengths L , $L + h$, and L , where the inner height of the stems is denoted by h .

For a rectangular parallelepiped $[0, L_x] \times [0, L_y] \times [0, L_z] \subseteq \mathbb{R}^3$, we have the following Neumann spatial eigenmodes which are separable:

$$\phi_{\vec{\alpha}}(\vec{r}) = \prod_{j=x,y,z} \sqrt{\frac{2}{L_j}} \cos\left(\frac{n_j \pi r_j}{L_j}\right), \quad (9a)$$

$$k^{(\vec{\alpha})} = \sqrt{\sum_{j=x,y,z} \left(\frac{n_j \pi}{L_j}\right)^2}, \quad (9b)$$

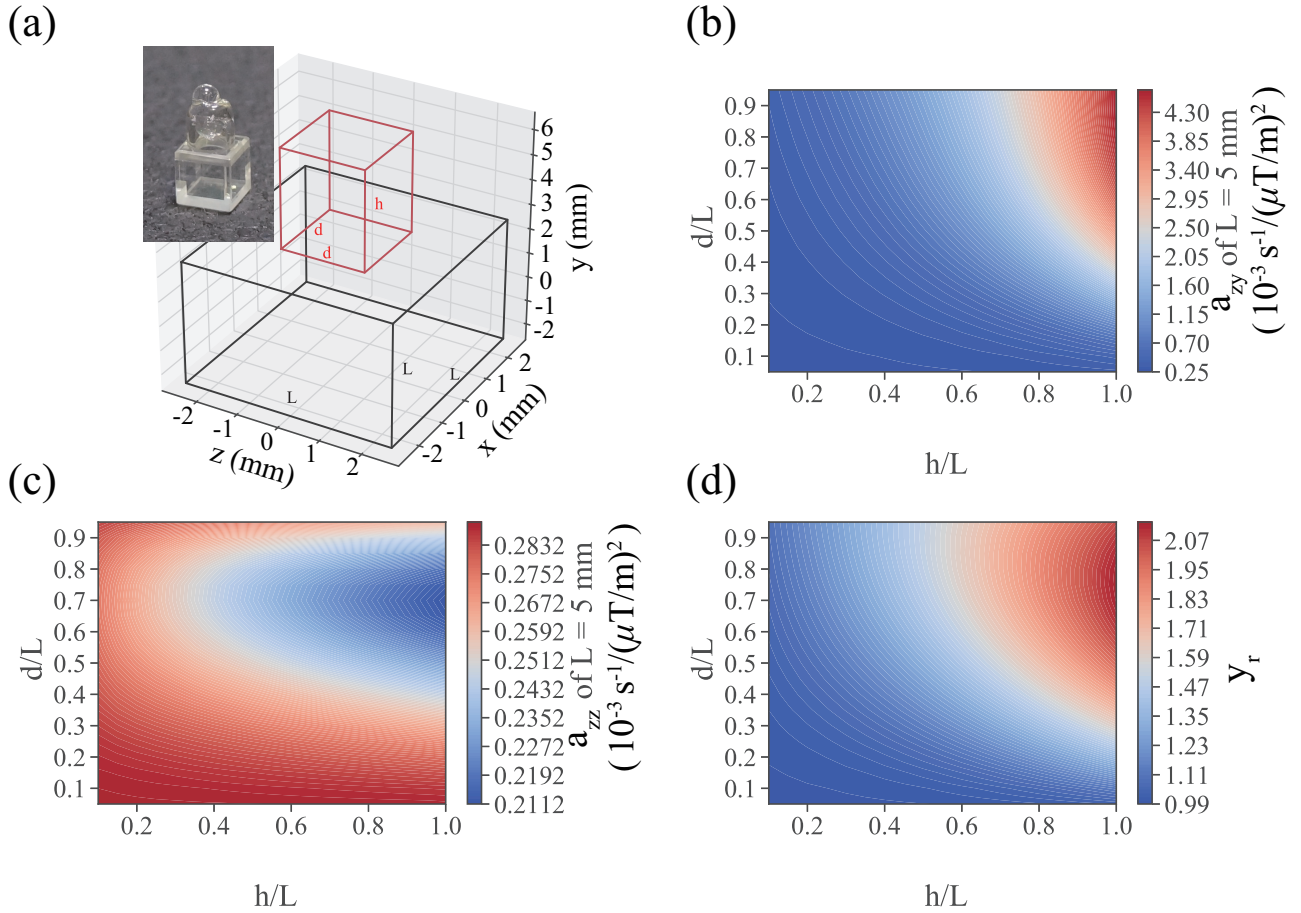


FIG. 1. (a) Model of the atomic gas cells. The solid line depicts the edges of the inner volume. The dimensions of the cubic part in the atomic gas cell are $5 \times 5 \times 5$ mm ($L = 5$ mm). The stem is modeled as a rectangular parallelepiped; h is the height and d is the width of the stem. The inset shows a picture of an atomic gas cell used in our experiment. (b) Quadratic coefficient, a_{zy} , as a function of the ratio of the stem width, d/L , and the ratio of the stem height, h/L , at $D = 1 \text{ cm}^2/\text{s}$ and $L = 5$ mm. (c) Quadratic coefficient, a_{zz} , as a function of the ratio of the stem width, d/L , and the ratio of the stem height, h/L , at $D = 1 \text{ cm}^2/\text{s}$ and $L = 5$ mm. (d) Ratio of quadratic coefficients, $y_r = (a_{zy}/a_{zz})^{1/4}$, as a function of the ratio of the stem width, d/L , and the ratio of the stem height, h/L . We note that the results of (b), (c), and (d) are numerically calculated.

where $n_j \geq 0$ and $\vec{r} = (x, y, z)$. The normalization constant $\sqrt{2/L_j}$ must be modified to $\sqrt{1/L_j}$ in case $n_j = 0$. We note that the lowest mode is the uniform mode which is given by $\phi_{0,0,0}(\vec{r}) = 1/\sqrt{L_x L_y L_z}$.

We now specialize to the case of a linear variation, i.e., $\vec{B}_{\text{inh}}(\vec{r}) = (\nabla \vec{B}_{\text{inh}})\vec{r} + \vec{b}$ for some constants $\nabla \vec{B}_{\text{inh}}$ and \vec{b} . Since the real part of $\Gamma_{0,11}^{(2)}$ gives the transverse relaxation rate, we get the following equation after applying the aforementioned formula for the spatial modes:

$$\begin{aligned} \Gamma_{\Delta B} &= \frac{\gamma^2}{120D} \sum_{j=x,y,z} L_j^4 \left| \frac{\partial B_z}{\partial r_j} \right|^2 \\ &+ \sum_{j=x,y,z} \sum_{n:\text{odd}} \frac{4\gamma^2 L_j^4 D}{\pi^2 n^2 (n^4 \pi^4 D^2 + \gamma^2 B_0^2 L_j^4)} \\ &\times \left[\left| \frac{\partial B_x}{\partial r_j} \right|^2 + \left| \frac{\partial B_y}{\partial r_j} \right|^2 \right]. \end{aligned} \quad (10)$$

We emphasize that the magnetic-field gradients are assumed to be constant throughout the cell. The first term in

Eq. (10) is much larger than the other term so that we can approximate $\Gamma_{\Delta B}$ as

$$\Gamma_{\Delta B} \approx \frac{\gamma^2}{120D} \sum_{j=x,y,z} L_j^4 \left| \frac{\partial B_z}{\partial r_j} \right|^2 = \sum_j a_{zj} \left| \frac{\partial B_z}{\partial r_j} \right|^2. \quad (11)$$

This shows that $\Gamma_{\Delta B}$ is a quadratic function of the B_z -field gradients and is more sensitive to the derivatives along axes corresponding to longer dimensions. Here, we defined the quadratic coefficients for $\partial B_z/\partial r_j$ as a_{zj} . We also define a quantity y_r as follows:

$$y_r = \left(\frac{a_{zy}}{a_{zz}} \right)^{1/4}. \quad (12)$$

Note that this definition coincides with the length ratio L_y/L_z in the case of the rectangular parallelepiped cell. In particular, $y_r = 1$ for cubic cells.

This quantity is important since it is not affected by scaling of the cells and changes in the diffusion coefficient. In order to show the invariance of y_r under the size scaling and the diffusion coefficient change, we calculate Eq. (8) for the special

case where the inhomogeneous fluctuation \vec{B}_{inh} is linearized, i.e., $\vec{B}_{\text{inh}}(\vec{r}) = (\nabla \vec{B}_{\text{inh}})\vec{r} + \vec{b}$ where $\nabla \vec{B}_{\text{inh}}$ and \vec{b} are constants:

$$\Gamma_{\Delta B} = \frac{g_K^2 \mu_B^2}{2\hbar^2} \text{Re} \left[\sum_{\beta \geq 1} \frac{(\nabla B_x \cdot \mathcal{I}_\beta)^2 + (\nabla B_y \cdot \mathcal{I}_\beta)^2}{D(k^{(\beta)})^2 - i \frac{g_K \mu_B B_0}{\hbar}} + 2 \sum_{\beta \geq 1} \frac{(\nabla B_z \cdot \mathcal{I}_\beta)^2}{D(k^{(\beta)})^2} \right], \quad (13)$$

where we assume ϕ_β are real-valued and $\mathcal{I}_\beta = \langle 0|\vec{r}|\beta \rangle = \int \vec{r} \phi_0(\vec{r}) \phi_\beta(\vec{r}) d^3\vec{r}$. Note that the constant offset vector \vec{b} does not appear in the final result. The first sum typically has a much larger denominator than the second term so that it can be ignored:

$$\Gamma_{\Delta B} \simeq \frac{g_K^2 \mu_B^2}{D\hbar^2} \sum_{\beta \geq 1} \frac{(\nabla B_z \cdot \mathcal{I}_\beta)^2}{(k^{(\beta)})^2}. \quad (14)$$

Because our analysis treats magnetic-field-gradient-induced interactions as perturbations, it describes the regime in which the diffusion rate (inverse of the diffusion time τ_D) is much larger than the perturbed Larmor frequency (inverse of the perturbed Larmor period τ_L):

$$\frac{1}{\tau_D} \approx \frac{D}{L_D^2} \gg \frac{1}{\tau_L} \approx \gamma |\nabla B| L_D, \quad (15)$$

where L_D is the diffusion length, roughly $L_D \approx L$. Our experiments are performed in this regime because the applied magnetic-field gradients ($|\nabla B|$) are very small in the order of nT/mm, and the size of the atomic gas cell (L) is also small in the order of mm.

Now we assume that the atomic cell domain is scaled with a factor of $\eta > 0$. The corresponding normalized spatial eigenmodes are given by

$$\phi_{\alpha'}(\vec{r}') = \phi_\alpha(\vec{r})/\sqrt{\eta^3}, \quad (16a)$$

$$k^{(\alpha')^2} = k^{(\alpha)^2}/\eta^2, \quad (16b)$$

where $\vec{r}' = \eta\vec{r}$ so that $\mathcal{I}'_\beta = \eta\mathcal{I}_\beta$. It leads to $\Gamma'_{\Delta B} = \eta^4\Gamma_{\Delta B}$ for fixed diffusion coefficient D . Therefore, $a'_{zj} = \eta^4 a_{zj}$ for $j = x, y, z$ so that y_r is invariant under the size scaling. Moreover, y_r is independent of D because a_{zj} are inversely proportional to D so that D is eliminated in a_{zy}/a_{zz} .

When the inner width of the stem is less than the dimension of the cube, i.e., $d < L$, y_r deviates from L_y/L_z because now the cell shape deviates from a simple rectangular parallelepiped so that the spatial eigenmodes are not separable. In this case, a numerical approach is required to calculate y_r correctly. Numerically calculated y_r values are given in the Appendix. We numerically calculated 20 eigenvalues and the corresponding eigenfunctions for various cell dimensions. By substituting these eigenvalues and eigenfunctions into Eq. (8), we can obtain the transverse relaxation rates.

In our numerical calculations, the dimension of the cubic part was $5 \times 5 \times 5$ mm, i.e., $L = 5$ mm. We calculated a_{zz} and a_{zy} for varying values of d/L and h/L between 0 and 1. When $d \approx L$ or zero, the numerically calculated results showed good agreement with the ones obtained analytically using Eq. (11). For example, when $d = 5$ mm and $h = 5$ mm, the analytical

solution gives $4.6275 \times 10^{-3} \text{ m}^2/(\text{s} \mu\text{T}^2)$ and the numerical calculation gives $4.6282 \times 10^{-3} \text{ m}^2/(\text{s} \mu\text{T}^2)$ at $D = 1 \text{ cm}^2/\text{s}$ for a_{zy} . Figures 1(b) and 1(c) show the numerically obtained quadratic coefficients by considering the model of the cell given in Fig. 1(a). Figure 1(d) shows the y_r values. As the width d of the stem increases, a_{zy} also increases; intuitively, large d implies large effective “ L_y ” in Eq. (11).

Our numerical analyses show a_{zz} that deviates by up to 26.9% from the analytically obtained value $\gamma^2 L_z^4/(120D)$ for the rectangular parallelepiped model, due to the effect of a stem on the spatial modes ϕ_α . From Eq. (14), we can deduce $a_{zz} \propto \sum_\beta |\langle 0|z|\beta \rangle|^2/(Dk^{(\beta)})^2$. When $d = L$, the spatial functions [see Eq. (9)] along the x and z directions in the cell are exactly those for a cubic with inner lengths L . a_{zz} becomes, therefore, the analytically obtained value $\gamma^2 L_z^4/(120D)$.

When $d < L$, the spatial functions along the x and z directions are now coupled with that along the y direction, which leads to a reduction in the contribution of $\partial B_z/\partial z$ and $\partial B_z/\partial x$ to $\Gamma_{\Delta B}$. Interestingly, a_{zz} attains its minimum at $d/L \simeq 0.7$, as shown in Fig. 1(c), so that we could reduce a_{zz} to be smaller than that of the cubic cell by adjusting the width of the stem.

In order to investigate the reduction of a_{zz} in the cell with a stem, we compare the largest term of $\sum_\beta |\langle 0|z|\beta \rangle|^2/(Dk^{(\beta)})^2$ in two cases: without a stem ($d/L = 0$) and with a stem ($d/L \simeq 0.7$). In the cell with a stem, the $\partial B_z/\partial z$ gradient coupling between the diffusion mode β and zero, given by $|\langle \beta|z|0 \rangle|$, is 1.4 times smaller than that in the cell without a stem. The corresponding spatial frequency $k^{(\beta)}$ in the cell with a stem is only 1.03 times larger than that without a stem. Therefore, the largest term of $\sum_\beta |\langle 0|z|\beta \rangle|^2/(Dk^{(\beta)})^2$ in the cell with a stem is about twice as small as the value in the cell without a stem, where the main contribution is $|\langle \beta|z|0 \rangle|^2$.

The coupling $|\langle \beta|z|0 \rangle|$ can be understood as the diffusion length L_D of the atom along the z direction. According to Eq. (15), as the diffusion length L_D becomes shorter, the diffusion rate D/L_D^2 becomes larger while the perturbed Larmor frequency $\gamma|\Delta B|L_D$ is getting smaller. As a result, motional narrowing along the z axis is enhanced in the cell with a stem. When the sum of higher spatial modes is considered, a_{zz} with a stem is 1.37 times smaller than that without a stem, corresponding to a deviation of 26.9%.

When $d \ll L$, the stem effect becomes small so that a_{zz} is recovered to the analytically obtained value $\gamma^2 L_z^4/(120D)$ for the rectangular parallelepiped model. Note that $\Gamma_{\Delta B}$ also includes cross-terms which are proportional to $\frac{\partial B_x}{\partial x} \frac{\partial B_z}{\partial y}$, $\frac{\partial B_x}{\partial x} \frac{\partial B_z}{\partial z}$, and $\frac{\partial B_z}{\partial y} \frac{\partial B_z}{\partial z}$ [see Eq. (14)]. These cross-terms are negligible since they were more than 500 times smaller than the main terms in our calculations: they even vanish for the case of rectangular parallelepipeds, as can be seen in Eq. (10).

The quadratic coefficients depend on temperature and pressure because the diffusion coefficient D is a function of temperature and pressure. Practically, the diffusion coefficient for a gas consisting of two kinds of molecules is determined by the following empirical equation developed by Fuller [18]:

$$D = \frac{10^{-3} T^{1.75} (1/M_A + 1/M_B)^{1/2}}{p [(\sum v_A)^{1/3} + (\sum v_B)^{1/3}]^2}. \quad (17)$$

Here, p is the total pressure (atm), M_A and M_B are molecular masses, $\sum v_i$ is the diffusion volume for component

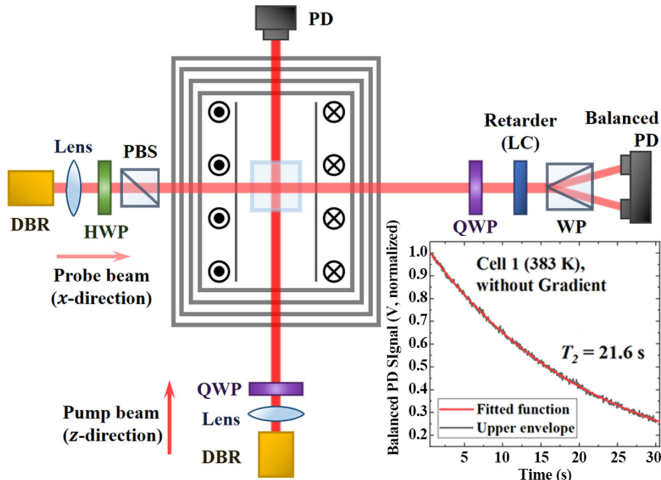


FIG. 2. Schematic diagram of the experimental setup. DBR, distributed Bragg reflector laser diode; HWP, half-wave plate; QWP, quarter-wave plate; PD, photodiode; LC, liquid crystal; WP, Wollaston prism. The inset shows the upper envelope of the FID signal and the exponential fitting, $y = A \exp(-t/T_2) + B$.

i , and T is the temperature (K). Relevant values are $\sum v_{\text{Xe}} = 37.9 \text{ cm}^3/\text{mol}$, $\sum v_{\text{N}_2} = 17.9 \text{ cm}^3/\text{mol}$, $M_{\text{Xe}} = 131.29 \text{ g/mol}$, and $M_{\text{N}_2} = 28.014 \text{ g/mol}$. For our atomic gas cells, we may use the ideal gas law because N_2 and Xe are nonpolar. Therefore, if the pressure during gas cell fabrication was p_0 at temperature T_0 , the pressure p at temperature T is roughly given by $\frac{p_0}{T_0} T$. As a result, the above-mentioned formula can be written as

$$D = \frac{CT_0 T^{0.75}}{p_0}, \quad (18)$$

where $C = \frac{10^{-3}(1/M_A + 1/M_B)^{1/2}}{[(\sum_A v_A)^{1/3} + (\sum_B v_B)^{1/3}]^2}$.

III. EXPERIMENTAL SETUP

The experimental setup is shown in Fig. 2. Details of the setup are given in Ref. [19], except for the description of the atomic gas cell. A four-layered magnetic shield (MS-2, Twinleaf) is adopted to attenuate external magnetic fields such as the Earth's magnetic field. A z -bias coil and gradient coils are built in on the inner surface of the magnetic shield. The z -bias coil generates a nearly homogeneous magnetic field of 92.3 nT/mA and the gradient coils generate 0.28 nT/(mm mA) for $\partial B_z/\partial z$, 0.253 nT/(mm mA) for $\partial B_z/\partial x$, 0.256 nT/(mm mA) for $\partial B_z/\partial y$, and 0.337 nT/(mm mA) for $\partial B_y/\partial y$.

The atomic gas cell is mounted on a structure made of polyether ether ketone and alumina (Al_2O_3). To heat up the atomic gas cell for effective spin-exchange optical pumping, an AC polyimide heater [20], which is designed to self-cancel the emitted magnetic field, is attached to the atomic gas cell. Moreover, a platinum resistor (PT1000) is also attached to the cell to measure the temperature of the cell.

A circularly polarized pump beam propagates along the z axis to polarize the Rb electron spins parallel to the z -bias field, and a linearly polarized probe beam propagates along the x axis, serving to detect the optical Faraday rotation. The

power of the pump beam was about 200 mW, and that of the probe beam was about 13 mW. The laser sources are 795-nm DBR lasers (PH795-DBR-160, Photodigm), where the frequencies were tuned to the D1 line of Rb.

To investigate the effect of stems, we prepared five different atomic gas cells of different dimensions. The inset of Fig. 1(a) is a photograph of an atomic gas cell used in our experiments. The inner length of the cube was 5 mm for atomic gas cells 1, 2, 3, and 4, and 10 mm for atomic gas cell 5. The thickness of the walls was 1.25 mm. Cells 1, 2, and 5 had stems with inner diameter $d = 4$ mm. The inner diameters of the stems were $d = 2$ mm in cell 3 and 4. Large d is advantageous for cell fabrication because the stem easily transfers the gas atoms into the cell. Although the stems are cylindrical, these are approximated as rectangular parallelepipeds for our calculations. Table II summarizes the dimensions of the five gas cells and the partial pressures of the gases in each cell. We note that cell 1 and 2 were attached to the same glass manifold, which was connected to a metallic atomic gas chamber during cell fabrication. We pinched off cell 1 and then cell 2 sequentially. Other cells were singly connected to the gas chamber. These cells were filled with natural Rb, ^{129}Xe , ^{131}Xe , N_2 , and H_2 of varying gas pressures via our cell fabricating system. After the gas-filling process, cells were pinched off manually with the help of a gas torch.

We performed the free induction decay (FID) measurement for five different atomic gas cells in the presence of various magnetic-field gradients. The inset of Fig. 2 shows the upper envelope of a normalized FID signal and the corresponding curve-fitted plot. The transverse relaxation time T_2 is obtained by curve fitting. In the fast diffusion limit, as expressed in Eq. (15), the fitting curve is given by the equation $y(t) = Ae^{-t/T_2} + B$ [11]. The transverse-spin-relaxation rate is given by $\Gamma_2 = 1/T_2$.

IV. RESULTS AND DISCUSSIONS

A. Quadratic coefficients of the transverse relaxation rate according to the magnetic-field gradients

Figure 3 shows the measured transverse relaxation rates as a function of applied B -field gradients $\partial B_z/\partial x$, $\partial B_z/\partial y$, and $\partial B_z/\partial z$ at the temperature of 368 K. The transverse relaxation rate can be written as $\Gamma_2 \approx \Gamma_{\Delta B} + \Gamma_{\text{col}} + \Gamma_{\text{wall}}$ where the B -field-gradient-induced transverse relaxation rate is given by $\Gamma_{\Delta B} = \sum_{j=x,y,z} a_{z,j} |dB_{\text{res},j} + \partial B_z/\partial r_j|^2$, where $dB_{\text{res},j}$ is the residual B -field gradient. The experimental data in Fig. 3 are well fitted by the quadratic function $y = a(x + x_c)^2 + b$. As shown in Fig. 3, the curvature of the transverse relaxation rate graph as a function of $\partial B_z/\partial y$ is much larger than that corresponding to $\partial B_z/\partial x$ and $\partial B_z/\partial z$ due to length extension provided by the stem. On the other hand, the two graphs corresponding to variables $\partial B_z/\partial x$ and $\partial B_z/\partial z$ are well overlapped because $L_x = L_z$ for the cell.

Table I shows the quadratic coefficients obtained from the curve fitting for five atomic gas cells at 365 K. To see the effect of the stems, we also showed the experimentally obtained $y_r^{(E)}$ which is defined as in Eq. (12). $y_r^{(E)}$ shows better agreement with the length ratios L_y/L_z for cases where $d \approx L$ ($d/L = 0.8$), as anticipated in the remark following

TABLE I. The measured quadratic coefficients for Γ_2 of ^{129}Xe in atomic gas cells at 365 K. Cell 1 and 2 were torn off by a blowtorch from the same glass branch, hence the asterisks. The numbers in round brackets represent the standard deviations. The (inner) length ratio L_y/L_z equals $(L+h)/L$ for the cell depicted in Fig. 1(a). $y_r^{(E)}$ (resp. $y_r^{(N)}$) denotes the experimentally (resp. numerically) obtained values of y_r .

Cell	a_{zz} [$\text{s}^{-1}/(\mu\text{T}/\text{m})^2$]	a_{zy} [$\text{s}^{-1}/(\mu\text{T}/\text{m})^2$]	a_{yy} [$\text{s}^{-1}/(\mu\text{T}/\text{m})^2$]	d/L	L_y/L_z	$y_r^{(E)}$	$y_r^{(N)}$
1*	2.89×10^{-4} (3.43×10^{-6})	5.72×10^{-3} (2.26×10^{-5})	3.83×10^{-5} (2.25×10^{-6})	0.8	2	2.12	2.14
2*	4.88×10^{-4} (7.50×10^{-6})	2.76×10^{-3} (4.46×10^{-5})	8.13×10^{-5} (2.56×10^{-6})	0.8	1.5	1.54	1.50
3	4.18×10^{-4} (4.06×10^{-6})	5.64×10^{-3} (1.81×10^{-4})		0.4	2	1.86	1.81
4	5.40×10^{-4} (3.24×10^{-6})	1.97×10^{-3} (1.15×10^{-4})		0.4	1.6	1.38	1.33
5	7.91×10^{-3} (8.63×10^{-5})	2.35×10^{-2} (1.41×10^{-3})		0.4	1.58	1.31	1.31

Eq. (12). As shown in Table I, $y_r^{(E)}$ deviates from L_y/L_z when $d/L = 0.4$ because the spatial modes are not separable. In this case, $y_r^{(E)}$ can be described by the numerical analysis based on the spatial modes in the cubic cell having the stem, instead of using the analytic formula L_y/L_z . The numerically calculated $y_r^{(N)}$ shows good agreement with $y_r^{(E)}$.

Comparing cell 4 and cell 5 gives some insight into the “scalability” of our results. These cells had similar d/L and h/L values: $d/L = 0.4$ and $h/L \approx 0.6$. On the other hand, the cube width L for cell 5 was 10 mm, which is two times larger than that of cell 4 so that all the length scales for cell 5 were two times larger than those of cell 4, i.e., $\eta = 2$. Therefore, the quadratic coefficients for cell 5 were expected to be $\eta^4 = 2^4 = 16$ times larger than those for cell 4. The measured value of $a_{zz}^{(\text{cell } 5)}/a_{zz}^{(\text{cell } 4)}$ was 14.6. This gap is reduced when the effect of the diffusion coefficients is considered. We note that the diffusion coefficient in cell 5 was slightly larger than that in cell 4 due to the difference in p_0 . (See Table II) If we estimate the diffusion coefficients by the Fuller formula, the theoretic ratio, which is given by $\eta^4[D^{(\text{cell } 4)}/D^{(\text{cell } 5)}]$, is 14.04.

In our analysis, we neglected terms originating from gradients of the transverse magnetic fields, i.e., $\partial B_x/\partial r_j$ and $\partial B_y/\partial r_j$. Assuming a typical value of $D = 0.6 \text{ cm}^2/\text{s}$, $L = L_x = L_y = L_z = 5 \text{ mm}$, and $B_0 = 10 \mu\text{T}$, we compare the two terms given in Eq. (10). The quadratic coefficient a_{zj} of the B_z -related terms and the quadratic coefficient $a_{xj} = a_{yj}$ of the $B_{x,y}$ -related terms are as follows ($j = x, y, z$):

$$a_{zj} = \frac{\gamma^2 L^4}{120D} = 4.80 \text{ cm}^2/\mu\text{T}^2, \quad (19)$$

$$a_{xj} = \sum_{n:\text{odd}} \frac{4\gamma^2 L^4 D}{\pi^2 n^2 (n^4 \pi^4 D^2 + \gamma^2 B_0^2 L^4)}$$

$$= 0.00275 \text{ cm}^2/\mu\text{T}^2.$$

The latter is 1745 times smaller than the former, which validates our approximation.

The measured a_{yy} in our experiments are, however, only about 5.25–6 times smaller than a_{zx} (or a_{zz}). This discrepancy is explained by the fact that $\nabla \cdot \vec{B}$ must vanish, so that a gradient $\partial B_y/\partial y$ necessarily induces the gradients, $\partial B_x/\partial x$

TABLE II. Characteristics of the atomic gas cells at temperature 365 K. D_F is calculated according to Eq. (17), whereas D_a is calculated using the relation $D = \gamma^2 L_z^4/(120a_{zz})$. D_n is the diffusion coefficient estimated from the numerical analysis of the cells, including the stem effect. Partial pressures of relevant gas species are given in the fifth column. For example, 8/48/150 indicates that 8 Torr of ^{129}Xe , 48 Torr of ^{131}Xe , and 150 Torr of $\text{N}_2\text{-H}_2$ mixture are injected into the cell at fabrication time. Cell 1 and 2 were torn off from the same glass branch by a fire torch. The numbers in round brackets represent the standard deviations.

Cell	L (mm)	d (mm)	h (mm)	Pressures (p_0) (Torr)	D_F (cm^2/s)	D_a (cm^2/s)	D_n (cm^2/s)
1*	5	4	5	8/48/150 (4% H_2)	0.526	0.986 (0.012)	0.752 (0.005)
2*	5	4	2.5	8/48/150 (4% H_2)	0.526	0.584 (0.009)	0.498 (0.008)
3	5	2	5	6/36/150 (4% H_2)	0.565	0.682 (0.007)	0.589 (0.006)
4	5	2	3	8/48/200 (4% H_2)	0.423	0.528 (0.003)	0.482 (0.003)
5	10	4	5.75	6/36/183 (14% H_2)	0.482	0.577 (0.006)	0.529 (0.006)

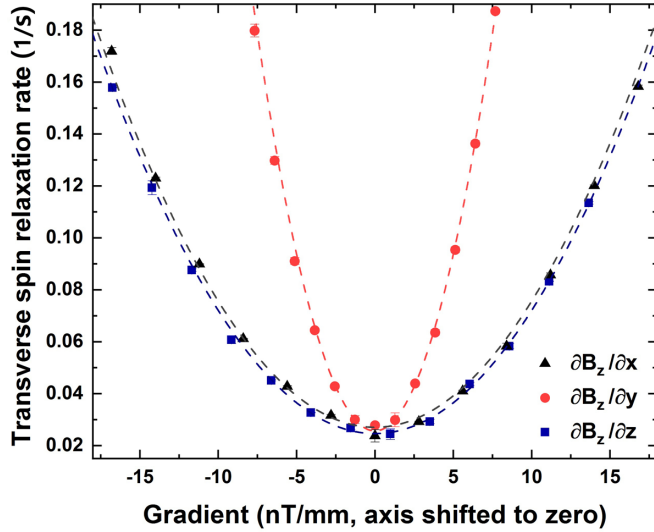


FIG. 3. Measured transverse relaxation rates ($\Gamma_2 = 1/T_2$) as a function of magnetic-field gradients, $\partial B_z/\partial z$ (blue squares), $\partial B_z/\partial x$ (black triangles), and $\partial B_z/\partial y$ (red circles) in cell 2. The dashed lines depict the quadratic curve fitting for the experimental data. The graphs were horizontally shifted so that the zero-point of the horizontal axis is on the axes of the quadratic curves.

and in particular $\partial B_z/\partial z$. We measured the magnetic-field gradients originating from our $\partial B_y/\partial y$ coil; -0.13 nT/(mm mA) for $\partial B_z/\partial z$ and -0.21 nT/(mm mA) for $\partial B_x/\partial x$ were induced when $\partial B_y/\partial y$ was applied with an efficiency of 0.34 nT/(mm mA) in the magnetic shield. As a result, $\partial B_z/\partial z \simeq -0.38 \partial B_y/\partial y$ in our setup so that effectively we had $a_{yy} \approx 0.38^2 a_{zz} = 0.1444 a_{zz}$ in the experiments. We got $a_{yy} \approx 0.19 a_{zz}$ in cell 1 and $a_{yy} \approx 0.17$ in cell 2, which seems reasonable. Similarly, $\partial B_z/\partial x$ (or $\partial B_z/\partial y$) also induces $\partial B_x/\partial z$ (or $\partial B_y/\partial z$) since $\nabla \times \vec{B} = 0$ in the cells. Again, contributions from this effect are typically small so that we can safely neglect them.

B. Diffusion coefficients of ^{129}Xe

We can extract the diffusion coefficient of ^{129}Xe in our cell from the measured a_{zz} by using Eq. (11), i.e., $D_a = \gamma^2 L^4 / (120 a_{zz})$. In a large atomic gas cell where the volume of the stem is relatively very small, the diffusion coefficient can be determined by using Eq. (11) [12,15]. However, D_a in a small cell can deviate from the real value because of the effect of the stem. In order to more precisely estimate the diffusion coefficient, we calculate Eq. (8) by substituting the diffusion coefficient of $1 \text{ cm}^2/\text{s}$ to obtain a_{zz} where the effect of the stem is incorporated. We can obtain D_n after dividing the measured a_{zz} by the calculated a_{zz} . We note that the diffusion coefficient estimated based on numerical eigenmode analysis, D_n , is smaller than D_a due to the effect of the stem. For comparison, we also estimated the diffusion coefficients using Fuller's equation Eq. (17), results of which are denoted as D_F . We neglected the effect of H_2 when applying Fuller's equation.

Table II summarizes our results. The pressures in Table II, p_0 , were measured at room temperature $T_0 = 293$ K. For cell 1 and cell 2, the measured diffusion coefficients are not in

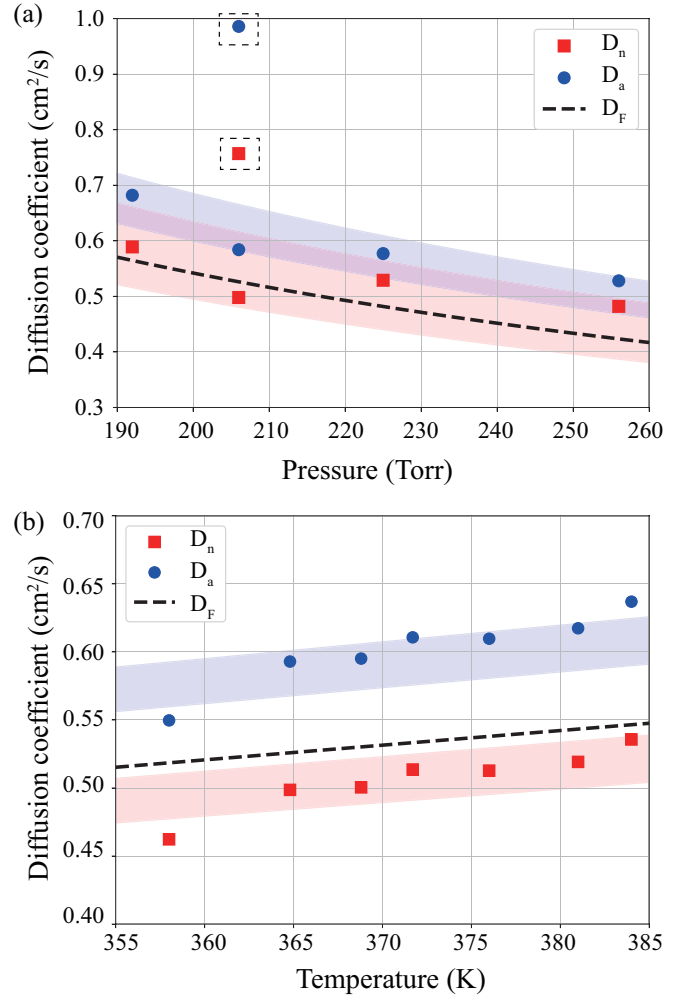


FIG. 4. (a) Diffusion coefficient as a function of total gas pressure. The red-filled squares denote diffusion coefficients estimated from the numerical analysis, D_n , and the blue-filled circles denote diffusion coefficients using the parallelepiped approximation, D_a . The black dashed line is the curve from Fuller's equation, $D = 108.4/p$, where D is in cm^2/s , and p is in Torr. The dashed rectangle indicates the excluded data in the fitting. The red shaded area (resp. blue shaded area) represents $D = (113 \pm 14)/p$ [resp. $D = (128 \pm 9)/p$], which is the result of the $D = a/p$ fitting. (b) Diffusion coefficient as a function of cell temperatures in cell 2. The black dashed line is the curve from Fuller's equation, $D = 0.0063T^{0.75}$ where D is in cm^2/s and T is in K. The red shaded area (resp. blue shaded area) represents $D = (0.0060 \pm 0.0002)T^{0.75}$ [resp. $D = (0.0070 \pm 0.0002)T^{0.75}$], which is the result of the $D = bT^{0.75}$ fitting.

accord with the calculation even though cell 1 and cell 2 were attached to the main gas chamber together. The measured diffusion coefficient of cell 1 was larger than the estimated value, while that of cell 2 was smaller than the estimated value. The pinch-off process using a gas torch locally heats the atomic gas cell, momentarily expanding the gas so that the precise determination of p_0 is disturbed. Moreover, an additional ambiguity may occur since the pressure gauge monitors the pressure in the main chamber, not the pressure in the atomic gas cell.

TABLE III. $y_r^{(N)}$ as a function of h/L and d/L . $0.05 \leq d/L \leq 0.5$.

$h/L \backslash d/L$	0.05	0.1	0.15	0.2	0.25	0.3	0.35	0.4	0.45	0.5
0.1	1.00037	1.00153	1.00356	1.00646	1.01021	1.01478	1.02015	1.02614	1.03267	1.03961
0.15	1.00059	1.00244	1.00565	1.01025	1.0162	1.02342	1.0319	1.04137	1.05166	1.0625
0.2	1.00086	1.00354	1.0082	1.01483	1.02337	1.03371	1.04572	1.05904	1.07343	1.08846
0.25	1.00119	1.00491	1.01132	1.02043	1.03208	1.04606	1.06218	1.0797	1.09857	1.11802
0.3	1.0016	1.00658	1.0152	1.02731	1.04267	1.06093	1.08161	1.10387	1.12747	1.15143
0.35	1.00212	1.00871	1.02001	1.03578	1.05554	1.07869	1.10449	1.13201	1.16048	1.1893
0.4	1.00276	1.01135	1.02596	1.04611	1.07098	1.09969	1.13111	1.16416	1.19773	1.23108
0.45	1.00356	1.01463	1.0333	1.05862	1.08937	1.12423	1.16162	1.2003	1.23887	1.2766
0.5	1.00458	1.01872	1.04218	1.07357	1.11099	1.15244	1.19628	1.24047	1.28395	1.32629
0.55	1.00584	1.02368	1.05291	1.09118	1.13589	1.1844	1.23469	1.28456	1.333	1.3794
0.6	1.00738	1.02972	1.06561	1.1117	1.16427	1.22003	1.27686	1.33213	1.38554	1.43592
0.65	1.00928	1.03698	1.08059	1.13513	1.19598	1.25916	1.32258	1.38328	1.44127	1.49487
0.7	1.01156	1.04558	1.09792	1.16166	1.23119	1.30173	1.37166	1.43765	1.4999	1.55681
0.75	1.01431	1.05571	1.11763	1.19128	1.26948	1.3477	1.42359	1.49451	1.56074	1.62073
0.8	1.01758	1.06742	1.14002	1.22383	1.31093	1.3964	1.47834	1.55404	1.62398	1.68638
0.85	1.02137	1.08087	1.16492	1.2592	1.35515	1.44783	1.53542	1.6158	1.6889	1.75401
0.9	1.0259	1.09615	1.19236	1.29742	1.40205	1.50171	1.5947	1.67935	1.75572	1.82315
0.95	1.03115	1.11334	1.22224	1.33804	1.45134	1.55756	1.65598	1.74492	1.82414	1.89358
1	1.03732	1.13249	1.25469	1.38108	1.50293	1.61589	1.71888	1.81166	1.89333	1.96513

To see if D_n is more accurate than D_a , we use Fuller’s equation as a benchmark. We rewrite Fuller’s equation as Eq. (18), where C is an absolute constant and $T_0 = 293$ K. In particular, $D = D(T, p_0) \propto 1/p_0$ for fixed T . In Fig. 4(a), we analyze the D_n -versus- p_0 and the D_a -versus- p_0 results tabulated in Table II by the fitting curve $D = a/p_0$. This gives us $a = 113 \pm 14$ for the D_n values and $a = 128 \pm 9$ for the D_a values. On the other hand, from Fuller’s formula we obtained $a = 108.4$, i.e., $D = 108.4/p_0$ at $T = 365$ K. We see that D_n is more accurate than D_a . This suggests that our numerical analysis incorporating the effect of the stem leads to better results. Here, we excluded the diffusion coefficients for cell 1

from the curve fitting process since these data points seem to be outliers.

In a similar vein, we also estimated the diffusion coefficient for cell 2 as a function of temperature. Figure 4(b) indicates that the diffusion coefficient increases with temperature, as one can easily expect. In view of Eq. (18), we expect that the diffusion coefficient is roughly proportional to $T^{0.75}$ for a fixed atomic gas cell so that the result was curve-fitted with $D = bT^{0.75}$. We obtained $b = 0.0060 \pm 0.0002$ by fitting the D_n values, whereas the D_a values gave us $b = 0.0070 \pm 0.0002$. On the other hand, we got $b = 0.0063$ from the Fuller equation Eq. (17). Again we see that D_F is closer to D_n than

TABLE IV. $y_r^{(N)}$ as a function of h/L and d/L . $0.55 \leq d/L \leq 0.95$.

$h/L \backslash d/L$	0.55	0.6	0.65	0.7	0.75	0.8	0.85	0.9	0.95
0.1	1.04677	1.05401	1.06118	1.0683	1.075	1.08119	1.08683	1.09189	1.09622
0.15	1.07364	1.08484	1.09591	1.10657	1.11635	1.12532	1.13301	1.1399	1.14549
0.2	1.10385	1.11905	1.13381	1.14784	1.16066	1.17216	1.18143	1.18965	1.1955
0.25	1.13754	1.15686	1.17523	1.19242	1.208	1.2209	1.23173	1.24028	1.24655
0.3	1.17537	1.19851	1.22021	1.24025	1.25805	1.27236	1.28423	1.29266	1.29796
0.35	1.21743	1.24401	1.26885	1.2915	1.31091	1.3264	1.33805	1.34586	1.34985
0.4	1.26309	1.29326	1.32089	1.34556	1.36612	1.38204	1.39334	1.40002	1.40221
0.45	1.31267	1.34615	1.37608	1.40232	1.42359	1.43954	1.44992	1.45501	1.45497
0.5	1.36599	1.40202	1.43407	1.46152	1.48303	1.4985	1.5076	1.51071	1.50806
0.55	1.42236	1.46104	1.49459	1.52274	1.54423	1.55884	1.56626	1.567	1.56142
0.6	1.48151	1.52234	1.55721	1.58587	1.60697	1.62016	1.62573	1.62382	1.61501
0.65	1.54323	1.58584	1.62185	1.65057	1.67097	1.68263	1.6859	1.68104	1.6688
0.7	1.60753	1.65157	1.68821	1.71667	1.73599	1.74603	1.74665	1.7386	1.72275
0.75	1.67354	1.71878	1.75583	1.78393	1.80205	1.81001	1.80781	1.79644	1.7768
0.8	1.7413	1.78756	1.82477	1.85226	1.8689	1.87458	1.8694	1.8545	1.83093
0.85	1.81052	1.8575	1.8949	1.92142	1.93641	1.93959	1.93132	1.91275	1.88516
0.9	1.88109	1.92869	1.9658	1.99128	2.00448	2.00488	1.99349	1.97112	1.93941
0.95	1.95261	2.00088	2.03755	2.06181	2.073	2.0708	2.05589	2.02963	1.99373
1	2.02533	2.07376	2.10999	2.13289	2.14191	2.13685	2.11842	2.08817	2.04806

TABLE V. a_{zz} as a function of h/L and d/L . a_{zz} is in $10^{-3} \text{ s}^{-1}/(\mu\text{T/m})^2$ units. $0.05 \leq d/L \leq 0.5$.

$h/L \backslash d/L$	0.05	0.1	0.15	0.2	0.25	0.3	0.35	0.4	0.45	0.5
0.1	0.289111	0.288799	0.288208	0.287331	0.286186	0.284776	0.283147	0.281462	0.279791	0.278149
0.15	0.289081	0.288663	0.287884	0.286731	0.285199	0.283319	0.281114	0.278766	0.276413	0.274087
0.2	0.289036	0.288516	0.287559	0.286159	0.284286	0.281995	0.279269	0.27638	0.273461	0.270548
0.25	0.288996	0.288367	0.287233	0.285585	0.2834	0.280723	0.277525	0.274221	0.270755	0.267305
0.3	0.288969	0.288236	0.286914	0.285027	0.282532	0.279481	0.2759	0.272138	0.268203	0.264266
0.35	0.288926	0.288079	0.286589	0.284455	0.281665	0.27826	0.274315	0.269998	0.265628	0.261154
0.4	0.288892	0.287931	0.286264	0.2839	0.280799	0.277047	0.272673	0.267933	0.26317	0.258363
0.45	0.288854	0.287787	0.285947	0.28334	0.279955	0.275853	0.271074	0.265984	0.261003	0.255802
0.5	0.28882	0.287642	0.28563	0.282776	0.279099	0.274653	0.269351	0.264091	0.258667	0.253079
0.55	0.288783	0.287505	0.285303	0.282219	0.278268	0.273485	0.267824	0.262262	0.256382	0.250425
0.6	0.288749	0.287363	0.284999	0.281673	0.277424	0.272306	0.266347	0.260483	0.25411	0.247745
0.65	0.288715	0.287215	0.284685	0.281115	0.276587	0.271137	0.264849	0.258626	0.251867	0.245353
0.7	0.288681	0.287076	0.284373	0.280575	0.27577	0.269987	0.26337	0.256774	0.249634	0.242802
0.75	0.288645	0.286938	0.284049	0.280029	0.274925	0.268853	0.261917	0.254912	0.247592	0.240433
0.8	0.288607	0.286789	0.283742	0.27949	0.274116	0.267719	0.260499	0.25312	0.24547	0.238086
0.85	0.288575	0.286647	0.283427	0.278942	0.273293	0.266603	0.259071	0.251321	0.24349	0.235815
0.9	0.288537	0.286505	0.283113	0.278406	0.272491	0.265488	0.25768	0.249632	0.241539	0.233601
0.95	0.288497	0.286362	0.282801	0.277869	0.271684	0.26438	0.256313	0.247826	0.23946	0.231427
1.0	0.288345	0.286223	0.282368	0.27723	0.270704	0.263104	0.254967	0.246149	0.237764	0.229286

D_a , which suggests that the stem effects must be taken into account.

In order to compare D_n with the diffusion coefficients obtained from the previous studies, we compensated the D_n values according to the pressure and temperature conditions given in Refs. [12,15]. By curve-fitting D_n in Fig. 4(a), we obtained $C = 0.0046 \pm 0.0006$ in Eq.(18) where $T_0 = 293$ K. Now, by substituting $C = 0.0046$ into Eq. (18), we obtain $D = 0.11 \text{ cm}^2/\text{s}$ at the standard temperature and pressure (STP) condition (760 Torr, 273 K). After the correction in-

cluding the diffusion coefficient of Xe in Xe gas [15], $D = 0.13 \text{ cm}^2/\text{s}$ is deduced. It shows a good agreement with the value in Ref. [12], $0.12 \text{ cm}^2/\text{s}$. At 760 Torr and 353 K, Ref. [15] reported $D = 0.21 \text{ cm}^2/\text{s}$. At the same condition, $D = 0.22 \text{ cm}^2/\text{s}$ is obtained from Eq. (18). We note that a temperature gradient within the mounted cell exists because our cell heater is in partial contact with the surface of the atomic gas cell. This nonuniformity of cell temperature, which induces convection, may have affected the diffusion coefficient measurements.

TABLE VI. a_{zz} as a function of h/L and d/L . a_{zz} is in $10^{-3} \text{ s}^{-1}/(\mu\text{T/m})^2$ units. $0.55 \leq d/L \leq 0.95$.

$h/L \backslash d/L$	0.55	0.6	0.65	0.7	0.75	0.8	0.85	0.9	0.95
0.1	0.276671	0.275515	0.274805	0.274564	0.274947	0.276063	0.277969	0.280701	0.284471
0.15	0.271979	0.270235	0.26903	0.268622	0.26915	0.270596	0.273405	0.277158	0.282436
0.2	0.267751	0.265548	0.264021	0.263466	0.263913	0.265516	0.269066	0.273654	0.280579
0.25	0.264128	0.261374	0.259531	0.258788	0.259093	0.261398	0.265185	0.270874	0.27858
0.3	0.260611	0.257587	0.255433	0.254509	0.254781	0.257293	0.261327	0.267881	0.276953
0.35	0.257138	0.25393	0.251491	0.250333	0.25071	0.253235	0.258017	0.265342	0.275504
0.4	0.254058	0.250442	0.247785	0.246468	0.246937	0.249695	0.254935	0.262979	0.274155
0.45	0.251003	0.24691	0.244157	0.242791	0.243388	0.246364	0.252043	0.260763	0.272895
0.5	0.247903	0.243734	0.240708	0.23927	0.240015	0.243236	0.249323	0.258692	0.271719
0.55	0.24503	0.240457	0.237382	0.23594	0.236779	0.240246	0.246761	0.256744	0.27062
0.6	0.242144	0.237471	0.234236	0.232755	0.23369	0.237394	0.244324	0.254904	0.269581
0.65	0.239469	0.234585	0.231096	0.229703	0.230742	0.234688	0.24201	0.253162	0.268603
0.7	0.23666	0.231605	0.228126	0.226767	0.227914	0.232112	0.239811	0.25151	0.267676
0.75	0.234062	0.228851	0.225324	0.223938	0.225211	0.229647	0.237719	0.249942	0.266804
0.8	0.231533	0.226169	0.222585	0.221211	0.222612	0.227286	0.235722	0.248452	0.265977
0.85	0.229069	0.223552	0.219882	0.218579	0.220113	0.22502	0.233819	0.247033	0.265185
0.9	0.226662	0.221029	0.217341	0.216034	0.217705	0.222834	0.232001	0.245685	0.264446
0.95	0.224286	0.218573	0.214849	0.213605	0.215391	0.220765	0.230253	0.244399	0.263734
1.0	0.221995	0.216189	0.212427	0.211227	0.213152	0.218765	0.228585	0.24317	0.263057

In order to precisely measure the frequency shift originating from the spin-spin interaction, the rotation, and the magnetic field, we need to maximize T_2 . For this, we may adjust $\partial B_z/\partial y$ and the temperature of the atomic gas cell. This is because $\Gamma_{\Delta B}$ is particularly sensitive to the partial derivative along the y axis (stem axis), as described in our theoretical analysis and experimental results (Fig. 3). Since there always exists a residual B -field gradient over the cell due to nonideal experimental conditions, we observe an increase in T_2 when the external $\partial B_z/\partial y$ is adequately applied to cancel this.

We also expect T_2 to increase with higher atomic gas cell temperatures since the diffusion coefficient increases with temperature. However, since the density of Rb gas increases with temperature, a larger Rb polarization-induced magnetic-field gradient due to optical pumping is generated [21–23]. Therefore, the effect due to diffusion competes with the effect of the Rb polarization-induced magnetic-field gradient, so that optimization of temperature is required to maximize T_2 .

V. CONCLUSION

We investigated the magnetic-field-gradient-induced transverse-spin relaxations of ^{129}Xe in sub-cm sized cubiclike atomic gas cells having stems. They were modeled as cubic cells on which rectangular parallelepiped stems are attached, where numerical eigenmode analyses are utilized to analyze the density-matrix equation with diffusion term. We compared the experimentally obtained quadratic coefficients

of the transverse-spin-relaxation rate from five different cells with the numerically calculated results.

We determined the ratio of quadratic coefficients y_r [see Eq. (12)], which is invariant under length scaling, and also determined the quadratic coefficients for $\Gamma_{\Delta B}$ at conditions $L_0 = 5$ mm and $D_0 = 1$ cm²/s (see the Appendix). One can estimate the quadratic coefficients in a cubic atomic gas cell with a rectangular parallelepiped stem by scaling our results $(L/L_0)^4(D/D_0)$ times. In addition, we determined the diffusion coefficient of ^{129}Xe , on the order of sub-cm²/s, using the experimentally obtained quadratic coefficients. The diffusion coefficient of ^{129}Xe at the STP condition was estimated to be $D = 0.13$ cm²/s.

ACKNOWLEDGMENT

This work was supported by a grant to Atom Optic Sensor Laboratory for National Defense funded by Agency for Defense Development.

APPENDIX

We provide $y_r^{(N)}$ and a_{zz} for conditions $D_0 = 1$ cm²/s and $L_0 = 5$ mm in Tables III–VI, which are calculated from our numerical eigenmode analyses. The quadratic coefficients of $\Gamma_{\Delta B}$ in an atomic gas cell with a stem can be estimated by scaling the provided results $(L/L_0)^4(D/D_0)$ times, where all the (inner) length scales are scaled by the factor of L/L_0 compared to the $L_0 = 5$ mm case.

-
- [1] M. Ebert, T. Grossmann, W. Heil, W. E. Otten, R. Surkau, M. Leduc, P. Bachert, M. V. Knopp, L. R. Schad, and M. Thelen, *Lancet* **347**, 1297 (1996)
 - [2] H.-U. Kauczor, R. Surkau, and T. Roberts, *Eur. Radiol.* **8**, 820 (1998).
 - [3] H. E. Möller, X. J. Chen, B. Saam, K. D. Hagspiel, G. A. Johnson, T. A. Altes, E. E. de Lange, and H.-U. Kauczor, *Magn. Reson. Med.* **47**, 1029 (2002).
 - [4] T. G. Walker and M. Larsen, *Adv. At. Mol. Opt. Phys.* **65**, 373 (2016)
 - [5] I. K. Kominis, T. W. Kornack, J. C. Allred, and M. V. Romalis, *Nature (London)* **422**, 596 (2003).
 - [6] J. M. Brown, S. J. Smullin, T. W. Kornack, and M. V. Romalis, *Phys. Rev. Lett.* **105**, 151604 (2010).
 - [7] J. Lee, A. Almasi, and M. Romalis, *Phys. Rev. Lett.* **120**, 161801 (2018).
 - [8] T. G. Walker and W. Happer, *Rev. Mod. Phys.* **69**, 629 (1997).
 - [9] G. B. Chavhan, P. S. Babyn, B. Thomas, M. M. Shroff, and E. M. Haacke, *Radio Graphics* **29**, 1433 (2009).
 - [10] G. D. Cates, S. R. Schaefer, and W. Happer, *Phys. Rev. A* **37**, 2877 (1988).
 - [11] W. Zheng, H. Gao, J.-G. Liu, Y. Zhang, Q. Ye, and C. Swank, *Phys. Rev. A* **84**, 053411 (2011).
 - [12] X. Liu, C. Chen, T. Qu, K. Yang, and H. Luo, *Sci. Rep.* **6**, 24122 (2016).
 - [13] D. D. McGregor, *Phys. Rev. A* **41**, 2631 (1990).
 - [14] S. D. Stoller, W. Happer, and F. J. Dyson, *Phys. Rev. A* **44**, 7459 (1991).
 - [15] K. C. Hasson, G. D. Cates, K. Lerman, P. Bogorad, and W. Happer, *Phys. Rev. A* **41**, 3672 (1990).
 - [16] J. Kitching, *Appl. Phys. Rev.* **5**, 031302 (2018).
 - [17] R. M. Noor, M. H. Asadian, and A. Shkel, *J. Microelectromech. Sys.* **29**, 25 (2020).
 - [18] E. N. Fuller, P. D. Schettler, and J. C. Giddings, *Ind. Eng. Chem.* **58**, 18 (1966).
 - [19] S. Lee, S. H. Yim, T. H. Kim, Z. Kim, and K. M. Shim, *J. Phys. B* **53**, 035502 (2020).
 - [20] S. H. Yim, Z. Kim, S. Lee, T. H. Kim, and K. M. Shim, *Rev. Sci. Instrum.* **89**, 116102 (2018).
 - [21] Z. Wang, J. Li, and Z. Xiong, *OSA Continuum* **3**, 903 (2020).
 - [22] L. Chen, B. Zhoua, G. Lei, W. Wu, Y. Zhai, Z. Wang, and J. Fang, *AIP Advances* **7**, 085221 (2017).
 - [23] D.-Y. Lee, S. Lee, and S. H. Yim, *Appl. Opt.* **60**, 7290 (2021).